ORIGINAL RESEARCH

Three-dimensional numerical analysis of the impact of the orientation of partially inclined baffles on the combined mass and heat transfer by a turbulent convective airflow

Jamal-Eddine Salhi[1] · Tarik Zarrouk[2] · Nassreddine Hmidi[1] · Merzouki Salhi[2] · Najim Salhi[2] · Mohammed Chennaif[3]

Abstract

This paper performed a three-dimensional numerical analysis of the flow structure and heat transfer enhancement of turbulent airflow through a rectangular channel (without baffles, with baffles). Two partially inclined baffles with different orientations are mounted on the bottom and top walls of the channel. The location of the baffles in the direction of flow through the channel of a heat exchanger is of great importance. It depends mainly on the geometrical parameters and the orientation of the baffles. Hence, our study focused on analyzing the effects of the baffles on the thermal–hydraulic behavior in the exchanger by choosing a flat baffle and four configurations of different orientations. Numerical results are presented in terms of axial velocity U, isotherms (T), turbulent kinetic energy (k), amount of heat dissipated by the channel surfaces (Q), average Nusselt number (Nu), friction factor (f), and thermal performance factor (η). The results show that the insertion of the partially inclined baffles into the channel causes the generation of vortices in the upstream and downstream areas of the baffle location point. Thus the mixing phenomenon occurs, which induces an increase in the heat transfer rate and generates a pressure drop simultaneously. Furthermore, the analysis of the results shows that compared to the smooth case (without baffles), the thermal performance factor (η) is significantly higher in the four configurations with baffles. Thus, for the different cases studied: (2); (3); (4); (5) and (6), the factor (η) is equal to 2.18; 2.16; 2.19; 2.27; and 2.25, respectively, for a Reynolds number equal to 87,300. The results also indicate that the transmitted relative heat quantities are equal to 116.08, 113.93, 118.2, 121.71, and 109.39%, respectively, for the same cases considered. Therefore, the configuration corresponding to case (5) performs better in heat transfer than the others. Finally, new correlations for predicting friction factor and Nusselt number as a function of Reynolds number and configuration are found at the end of this study.

Keywords Heat transfer · Numerical analysis · Turbulent flow · Heat exchangers · SIMPLE algorithm · Computational Fluid Dynamics

Abbreviations

f	Friction factor
D_h	Hydraulic diameter, [m]
h	Baffle height, [m]
H	Channel height, [m]
K	Turbulent kinetic energy [m/s^2]
L	Channel length, [m]
Nu	Local Nusselt number
L_2	Distance between the two baffles, [m]
T	Temperature, [K]
T_{int}	Temperature at inlet, [K]
T_w	Wall temperature, [K]
UV	Velocity components, [m/s]
U_{int}	Velocity at inlet, [m/s]
xy	Cartesian coordinates, [m

Greek Symbols

Φ	Inclination angle [degree]
δ	Baffle thickness, [m]
λ_f	Fluid thermal conductivity, [W.m^{-1}.K^{-1}]
ρ	Air density [kg/m^3]

✉ Jamal-Eddine Salhi
    j.salhi@ump.ac.ma

1   Équipe Des Sciences Des Matériaux, Laboratoire LPTPME, Département de Physique, Énergies Nouvelles Et Applications, Université, Faculté des sciences, Mohammed 1er, 60000 Oujda, Morocco

2   Faculty of Sciences, First Mohammed University, 60000 Oujda, Morocco

3   Laboratory of Electrical Engineering and Maintenance – LEEM, High School of Technology, University Mohammed 1st, Oujda, Morocco

μ_t	Turbulent viscosity, [Pa.s]
τ	Shear stress, [Pa]
ϕ	Stands for the dependent variables u, v, T, k and ε
ε	Dissipation rate [m/s^2]

Subscripts

FVM	Finite volume method
Int	Inlet
Low	Lower
Up	Upper
b	Baffle
s	Smooth channel
int	Inlet
out	Outlet

Introduction

Heat exchangers are systems whose operation is based on the exchange and the heat/energy transfer between two or more media imperiled to different temperatures. These exchangers represent an essential element having some primordial applications in several sectors like the industrial, transportation, residential sector, and others. Therefore, the enhancing the performances of these exchangers became a necessity to a better control and management of this heat energy. This development should necessary pass through the developing the heat and present configurations able to provide better thermal efficiency.

Indeed, to design high-performance heat exchangers, many researchers have dedicated to study the phenomena, thermal and hydrodynamic, to improve their performance in heat transfer. Among the topics studied, the improvement in thermo-solar systems occupies a large place [1–8].

Generally, to improve the performance of a heat transfer system two different ways are used: (i) increasing the thermal viscosity of its cooling fluid or (ii) by changing the flow structure of the heat transfer (cooling) fluid. In the first mode, the technique substitutes a fluid with a higher thermal conductivity for the cooling fluid. While the second consists on the integration of baffles vortex generators that favor the phenomenon of turbulence. In this paper, we will focus on the second technique. But before dealing with the methodology and the innovation of this paper a literature review will be discussed. In fact, to improve the rate of exchange and heat transfer by convection, many researchers have used baffles [9–12] or ribs as inserts to reduce the thickness of the thermal boundary layer and improve the heat transfer [13–18]. In the same context, Kelkar et al. [19] presented a numerical study of forced convective heat transfer in ducts with periodically varying cross-sectional areas. Similarly, Maakoul et al. [20] numerically examined the thermal–hydraulic

performance of STHXs with helical, segmental, and tri-lobed hole baffles. Lei et al. [21] investigated the effect of helix angles on overall characteristics and concluded that 45° is the most advantageous. Also, Sahel et al. [22] used a numerical models to assess the influence of hole location (PAR) on perforated baffles. According to Sara et al. [23], using solid ribs with a 90° angle of attack to the axial flow resulted in heated zones. Recently, several studies have used the V-shape concept ribs, for instance Chai et al. [24] looked at the influence of rib form in channels, comparing rectangular, front triangular, rear triangular, isosceles triangular, and semicircular ribs. Furthermore, Chang et al. [25] improved a channel heat exchanger's thermal–hydraulic performance by adding oblique baffles and perforated slots. TPF was raised to 3.4–2 and 3.2–1.6 for Reynolds numbers 10,000 to 50,000. Based on the TPF values, the authors recommended oblique slots downstream of bordering oblique ribs.

On the other hand, Vashistha et al. [26] examined a circular tube's fluid flow and thermal behavior with multiple counter-flow inserts. Gunes et al. [27] discovered excellent overall enhancement efficiency in turbulent flow in a circular tube with a free spiral wire inserted with three-pitch ratios and two distances. Demartini et al. [28] analyzed turbulent airflow in a rectangular duct with two baffles. The selected shape is a simple tubular heat exchanger baffle geometry. This research demonstrates that the pressure and velocity fields are most variables around the baffles. Feijó et al. [29] offered a geometric optimization of a channel heated by various chemicals on the top and bottom sides. Also, Bazdidi-Tehrani et al. [30] simulated laminar fluid flow and heat transfer in a two-dimensional horizontal channel with in-line baffles. They found that V-baffles are inefficient due to Reynolds number and blocking ratio for high blocking ratios.

In the present study, we presented a novel concept of ribs integration and optimize them to enhance the heat transfer inside a cannel. These integrations have as objective increasing the turbulent, convective and forced flow of a heat transfer fluid. The concept is proposed by two partially inclined baffles, with different orientations. Moreover, our objective is to make a three-dimensional analysis and study the effect of the orientation of the baffles about the direction of flow on the thermohydrodynamic phenomenon and to seek the optimal position corresponding to the maximum rate of heat transfer with a minimum of pressure loss. The thermo-aerodynamic characteristics are listed below:

- Aerodynamic characteristics are streamlines, axial velocity (U), turbulence kinetic energy distribution (K), and friction factors (f).
- Thermal characteristics are isotherms, average Nusselt number (Nu), amount of heat transmitted by the system (Q), and fluid temperature profiles (T).

- The thermo-aerodynamic characteristic is the thermal performance enhancement factor (η).

Finally, a benchmark of the thermal performance of our proposed model has been conducted with other rib shapes already published in the literature. The results show that our proposed ribs configuration can enhance the thermal performances by around 48% in comparison to the V-Shape ribs. Which proofs the performance of the novel proposed configuration on enhancing the thermal transfer in heat exchangers.

Physical model

The geometry of the problem studied is illustrated in Figs. 1 and 2. Figure 1a represents a three-dimensional schematic diagram of a smooth rectangular section channel model, which is placed horizontally and traversed by a heat transfer fluid's turbulent, convective, and forced flow. Figure 1b illustrates the experimental and numerical model studied by [28], a horizontally placed rectangular section channel containing two straight baffles installed on its lower and upper walls.

To intensify the heat exchange, it is necessary to modify the flow structure by creating recirculation zones to ensure good mixing and increase the heat exchange rate between the heat transfer fluid and the exchange surfaces.
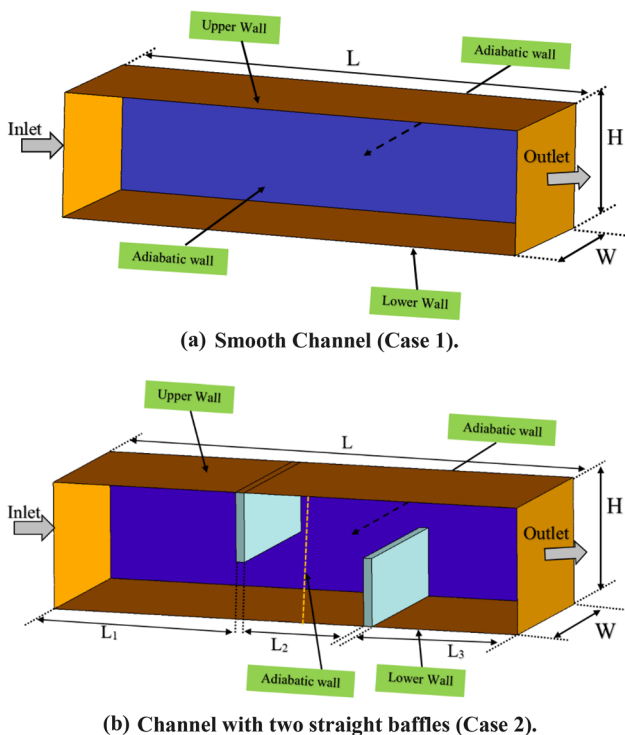

(a) Smooth Channel (Case 1).

(b) Channel with two straight baffles (Case 2).

Fig. 1 The schematics of the: **a** Smooth Channel (without baffles); **b** Channel with two straight baffles

The choice of the studied heat exchanger model, presented in Fig. 2, was made based on experimental and numerical data from [28]. The new model is characterized by the insertion of two partially inclined baffles (see Fig. 3), which can have different orientations and are adiabatic. The physical properties of the considered heat transfer fluid (air) have been kept for all the analysis cases and are illustrated in Table 1. All the required details on the geometrical parameters are provided in Table 2.

In the cases of Fig. 2, which follow, the conduit is in the presence of differently inclined baffles.

Mathematical formulation of the problem

The present numerical model is designed based on the following assumptions:

- Three-dimensional steady-state flow.
- The fluid is Newtonian, incompressible and turbulent flow;
- Fluid properties are assumed to be constant.
- Viscous dissipation and radiation are negligible.
- The Baffles are considered as adiabatic walls;
- The axial velocity and temperature at the entrance of the channel are uniform;
- The walls (upper and lower) are maintained at constant temperature;

Fluid flow and heat transfer procedures must obey the laws of conservation of mass (1), momentum (2)-(4) and energy (5).

These governing equations are described as follows [35]:

- The continuity equation [35]:

$$\frac{\partial(\rho u)}{\partial x} + \frac{\partial(\rho v)}{\partial y} + \frac{\partial(\rho w)}{\partial z} = 0 \tag{1}$$

- The momentum equation [35]:

$$\frac{\partial(\rho u^2)}{\partial x} + \frac{\partial(\rho uv)}{\partial y} + \frac{\partial(\rho uw)}{\partial z} = -\frac{\partial P}{\partial x} + \frac{\partial}{\partial x}\left[(\mu_l + \mu_t)(\frac{\partial u}{\partial x})\right] \\ + \frac{\partial}{\partial y}\left[(\mu_l + \mu_t)(\frac{\partial u}{\partial y})\right] + \frac{\partial}{\partial z}\left[(\mu_l + \mu_t)(\frac{\partial u}{\partial z})\right] \tag{2}$$

$$\frac{\partial(\rho uv)}{\partial x} + \frac{\partial(\rho v^2)}{\partial y} + \frac{\partial(\rho wv)}{\partial z} = -\frac{\partial P}{\partial y} + \frac{\partial}{\partial x}\left[(\mu_l + \mu_t)(\frac{\partial v}{\partial x})\right] \\ + \frac{\partial}{\partial y}\left[(\mu_l + \mu_t)(\frac{\partial v}{\partial y})\right] + \frac{\partial}{\partial z}\left[(\mu_l + \mu_t)(\frac{\partial v}{\partial z})\right] \tag{3}$$
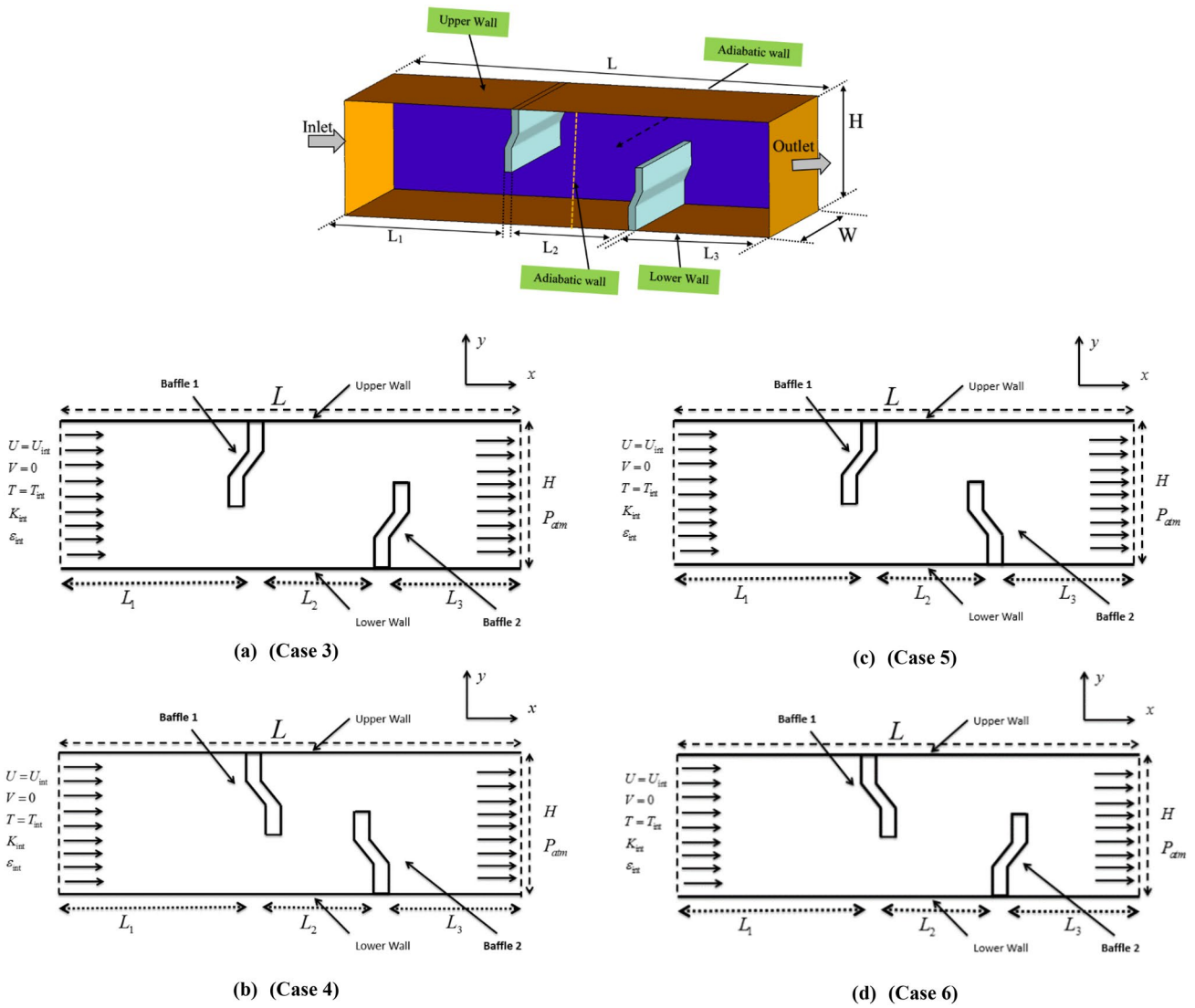
Fig. 2 Schematic of the different configurations studied with different orientations
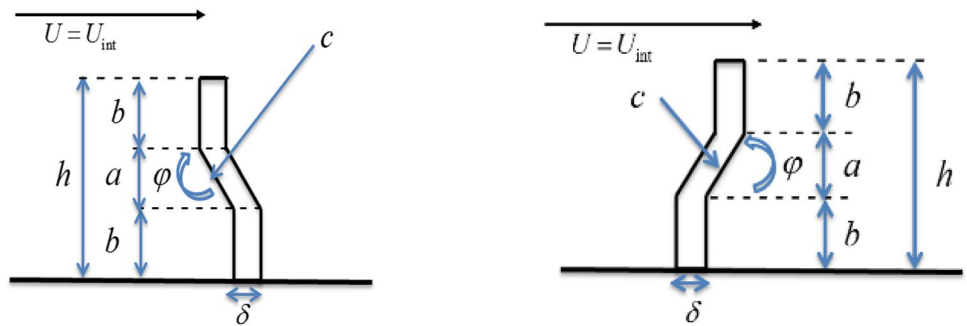
Fig. 3 dimensions of the baffle

Table 1 Properties of air as a function of temperature [34]

Coefficient	$a_1 + a_2 \times T + a_3 \times T^2 + a_4 \times T^3 + a_5 \times T^4$			
Properties of air	ρ (kg/m³)	C_p (J/(kg.K))	μ(kg/(m.s))	λ(W/(m.K))
a_1	4.5399557047065677	1.0540764984602797E+3	9.4680032779877928E-5	1.8028147194179223E-2
a_2	-2.3244292640615217E-2	-3.5067618164922393E-1	-1.0222587861878098E-6	-1.6851766935888901E-4
a_3	5.6404522707476041E-5	5.8416753365658986E-4	4.7054455296163551E-9	1.3838388187738584E-6
a_4	-6.2803748539876179E-8	3.0329858178609656E-7	-9.1119064881185846E-12	-3.2630462746304979E-9
a_5	2.3678170919661321E-11	-5.2479296621138882E-10	6.5461225665736524E-15	2.7514584927209003E-12

Table 2 Details of the dimensions of the physical problem [28]

Parameters	Values
L(m)	0.554
H(m)	0.146
L_1(m)	0.218
L_2(m)	0.142
L_3(m)	0.174
δ(m)	0.01
Φ (degré)	65°
c.sin(φ)	0.02
b(m)	0.03
W(m)	0.097
h(m)=2b+c.sin(φ)	0.08

Table 3 The empirical constants of the model k-ε [31, 32]

$C_{1\varepsilon}=C_{3\varepsilon}$	$C_{2\varepsilon}$	C_{μ}	σ_k	σ_ε
1.44	1.92	0.09	1.0	1.3

Where μ_t is the turbulent viscosity and is written as : $\mu_t = \rho c_\mu k^2 / \varepsilon$ (8)

The empirical constants of the model k-ε are mentioned in Table 3 below:

$$\frac{\partial(\rho uw)}{\partial x} + \frac{\partial(\rho vw)}{\partial y} + \frac{\partial(\rho w^2)}{\partial z} = -\frac{\partial P}{\partial z} + \frac{\partial}{\partial x}\left[(\mu_l + \mu_t)(\frac{\partial v}{\partial x})\right] + \frac{\partial}{\partial y}\left[(\mu_l + \mu_t)(\frac{\partial v}{\partial y})\right] + \frac{\partial}{\partial z}\left[(\mu_l + \mu_t)(\frac{\partial v}{\partial z})\right]$$ (4)

- The energy equation [35]:

$$\frac{\partial(\rho uT)}{\partial x} + \frac{\partial(\rho vT)}{\partial y} + \frac{\partial(\rho wT)}{\partial z} = \frac{\partial}{\partial x}\left[(\mu_l + \frac{\mu_t}{\sigma_T})(\frac{\partial T}{\partial x})\right] + \frac{\partial}{\partial y}\left[(\mu_l + \frac{\mu_t}{\sigma_T})(\frac{\partial T}{\partial y})\right] + \frac{\partial}{\partial z}\left[(\mu_l + \frac{\mu_t}{\sigma_T})(\frac{\partial T}{\partial z})\right]$$ (5)

The k-ε model [31, 32] was chosen to describe the turbulence phenomenon and the SIMPLE algorithm [33] is used to overcome the pressure–velocity coupling problem.

For the kinetic energy of turbulence (k) [35]:

$$\frac{\partial(\rho uk)}{\partial x} + \frac{\partial(\rho vk)}{\partial y} + \frac{\partial(\rho wk)}{\partial z} = \frac{\partial}{\partial x}\left[(\mu_l + \frac{\mu_t}{\sigma_k})(\frac{\partial k}{\partial x})\right] + \frac{\partial}{\partial y}\left[(\mu_l + \frac{\mu_t}{\sigma_k})(\frac{\partial k}{\partial y})\right] + \frac{\partial}{\partial z}\left[(\mu_l + \frac{\mu_t}{\sigma_k})(\frac{\partial k}{\partial z})\right]$$ (6)

For the dissipation rate of kinetic energy (ε) [35]:

$$\frac{\partial(\rho u\varepsilon)}{\partial x} + \frac{\partial(\rho v\varepsilon)}{\partial y} + \frac{\partial(\rho w\varepsilon)}{\partial z} = \frac{\partial}{\partial x}\left[(\mu_l + \frac{\mu_t}{\sigma_\varepsilon})(\frac{\partial \varepsilon}{\partial x})\right] + \frac{\partial}{\partial y}\left[(\mu_l + \frac{\mu_t}{\sigma_\varepsilon})(\frac{\partial \varepsilon}{\partial y})\right] + \frac{\partial}{\partial z}\left[(\mu_l + \frac{\mu_t}{\sigma_\varepsilon})(\frac{\partial \varepsilon}{\partial z})\right]$$ (7)

Boundary conditions

Solving the system of equations governing the physical problem requires incorporating boundary conditions for each dependent variable.

- At the inlet of the channel

$$U = U_{int}; V = 0; W = 0; T = T_{int}$$ (9)

- At the walls (upper and lower)

$$U = V == W = 0; and\, T = T_w;$$ (10)

- At the solid liquid interface

$$\lambda_f \frac{dT_f}{\delta n}\Big)_{\vec{N}} = \lambda_s \frac{dT_s}{\delta n}\Big)_{\vec{N}}, \; and \; T_f\big|_{\vec{N}} = T_s\big|_{\vec{N}}$$ (11)

- At the exit

$$\frac{\partial \phi}{\partial x} = 0; \; \phi = U, V, W, T, k, \varepsilon; \; and \; P = P_{atm},$$ (12)

The formula defines the main parameters of the current investigation:

- The Reynolds number is a dimensionless parameter that is defined as follows [35]:

Table 4 Convergence criterion for normalized residuals for the flow and energy equations

Convergence criterion	Continuity equation	Energy equation	k-equation	ε-equation	Velocity equation-x	Velocity equation-y	Velocity equation-z
Values	10^{-4}	10^{-9}	10^{-6}	10^{-6}	10^{-6}	10^{-6}	10^{-6}

$$\mathrm{Re} = \frac{\rho U_{\mathrm{int}} D_h}{\mu} \tag{13}$$

- The friction factor (f) [34]:

$$f = \frac{2}{\left(\frac{L}{D_h}\right)} \times \frac{\Delta P}{\rho U_m^2} \tag{14}$$

- Average Nusselt Number (Nu_{Avg}) [34]:

$$Nu_{avg} = \frac{hD_h}{\lambda} \tag{15}$$

- The heat flux dissipated by the hot surface can assumed equal to that evacuated by convection into the fluid as [35]:

$$Q = \dot{m}\, C_p \left(T_{out} - T_{\mathrm{int}}\right) = hA(T_w - T_b) \tag{16}$$

- The thermal enhancement factor (η) is defined by [35]:

$$\eta = \left(Nu/Nu_0\right) \Big/ \left(f/f_0\right)^{\frac{1}{3}} \tag{17}$$

The average Nusselt number (Nu) and the friction factor (f) are normalized by the Dittus–Boelter and Blasius correlation.

For a smooth channel [37, 38].

Dittus–Boelter correlation [37]:

$$Nu = 0.023 \mathrm{Re}^{0.8} \mathrm{Pr}^{0.4} \quad \mathrm{For}\, 10^4 \leq \mathrm{Re} \tag{18}$$

Blasius correlation [38]:

$$f = 0.3164 \mathrm{Re}^{\frac{-1}{4}} \quad \mathrm{For}\, 2 \times 10^3 \leq \mathrm{Re} \leq 10^5 \tag{19}$$

Numerical procedure

The numerical calculation is implemented by ANSYS Fluent 19.0 [39], and the governing equations are discretized and solved based on the finite volume method, the SIMPLE algorithm [34] is selected to handle the coupling between velocity and pressure. The convective terms of the governing equations are discretized by adopting the QUICK scheme [36]. The convergence criterion for the normalized residuals is shown in Table 4 for the flow and energy equations.
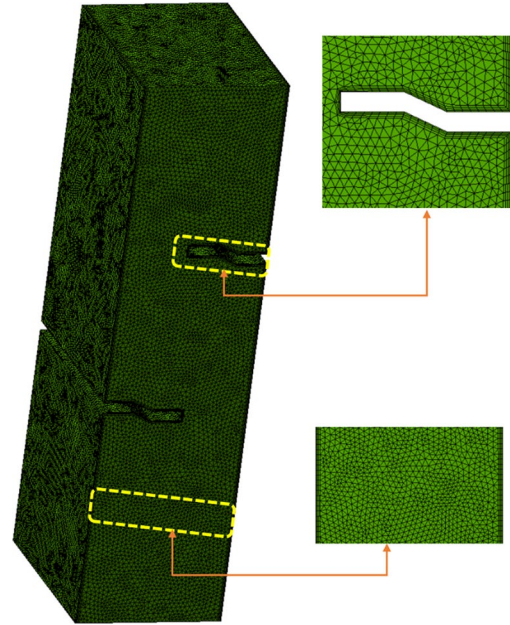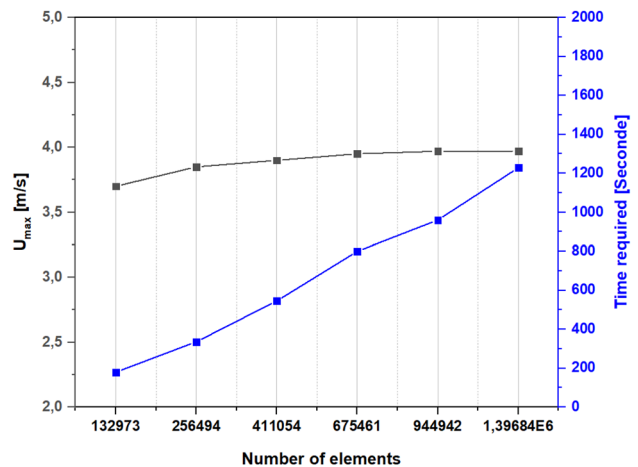

Fig. 4 Mesh of the study area

Fig. 5 Variation of axial velocity as a function of cell number

Mesh independence

In order to determine the grid offering the best accuracy with a reduced computation time, various grid sensitivity tests were performed for a Reynolds number equal to

Re = 10 000. Knowing that the value of the mean Nusselt number depends on the chosen mesh, then to study its sensitivity to the number of cells of a mesh (Fig. 4), the tests were carried out on six different grids, as indicated in Fig. 5. Moreover, it could notice that the values of the average Nusselt number change with the change of the mesh. However, beyond grid 944,942, this sensitivity becomes negligible; between grid 944,942 and grid 1,396,842, the calculated maximum axial velocity difference is less than 0.0002 = 0.02%. The 944,942 grid can therefore be considered the most optimal and chosen to perform all calculations in our study. The simulations were performed on a computer with an Intel Xeon Duo 3.4 GHz processor and 64 GB of RAM. The convergence was obtained after 7000–10,000 iterations.
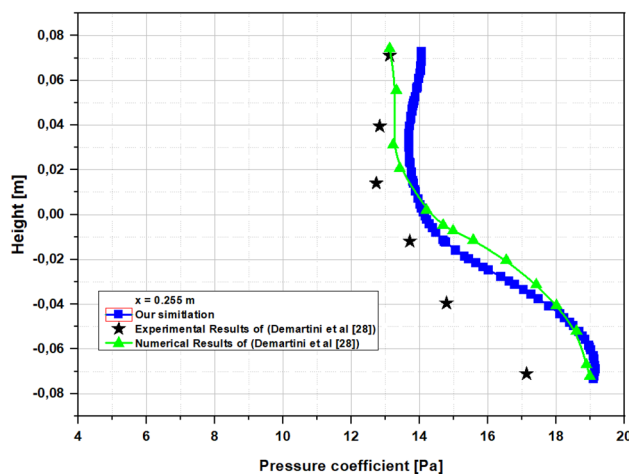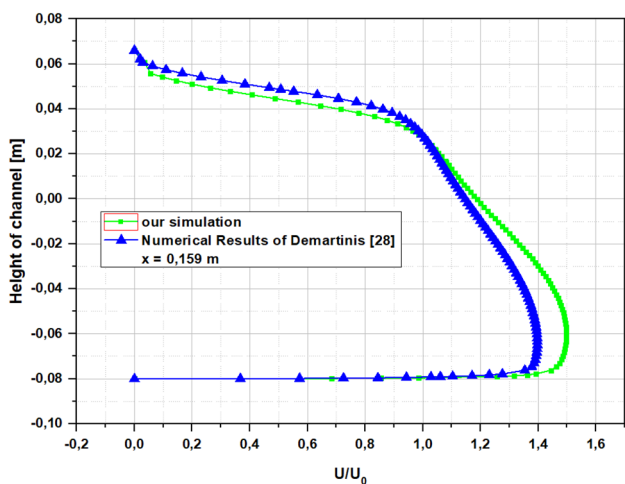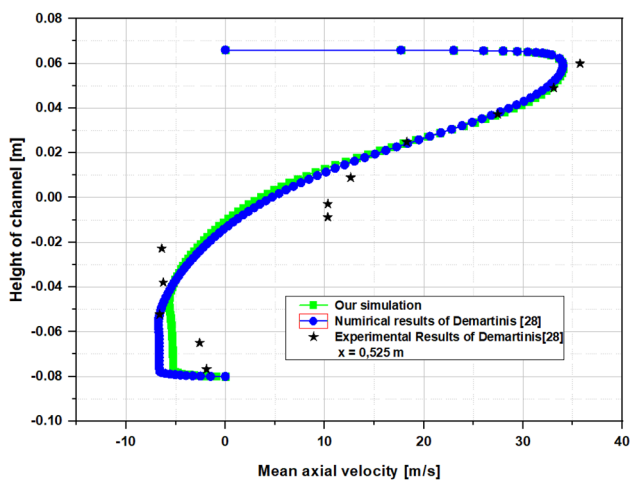

Fig. 7 Variation of the pressure coefficient along with the channel height

Numerical validation

Figure 6a-b shows the results of the velocity profiles along the channel height obtained by our (numerical) simulation and those obtained by numerical approach by Demartini et al.[28], at the two particular positions, respectively, $x_1 = 0.159$ m and $x_2 = 0.525$ m.

Figure 7 shows the excellent agreement of our simulated results and those calculated by numerical approach at position x = 0.255 m, presented in the paper [28], for the variation of the pressure coefficient along with the channel height.

Verification for the case of a smooth rectangular channel

The working fluid used is air. The inlet velocity is given in Reynolds number (Re), ranging from 10,000 to 87,300. The Nusselt number (Nu) and the friction factor (f) are the quantities chosen to analyze the characteristics of the airflow structure in the considered physical space (smooth rectangular channel), of the heat transfer, as well as the losses in the flow by friction. The calculated values of Nu and f were compared with those obtained from the Dittus–Boelter (Eq. (18)) and Blasius (Eq. (19)) correlations under identical operating considerations. As shown in Fig. 8, the calculated results agree pretty well in the ranges of 2.5% and 1.15% for the Nusselt number and Dittus–Boelter correlation, and for the friction factor and Blasius correlation, respectively.

In conclusion, it can say that the developed numerical scheme is quite reliable and can be used to predict the turbulent flow in forced convection within the whole studied domain.
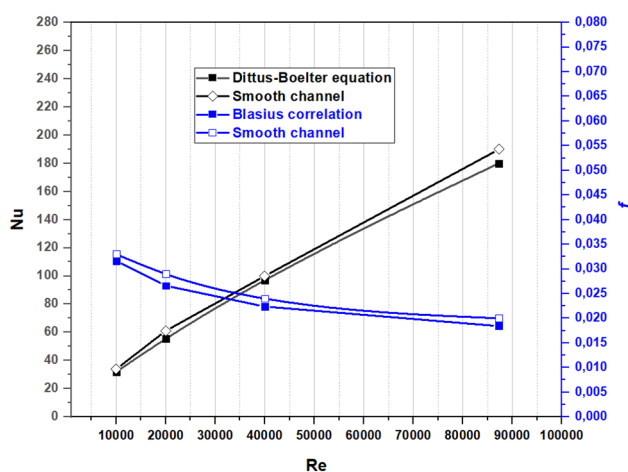

(a)

(b)

Fig. 6 Axial velocity at $x_2 = 0.525$ m, for experimental and numerical results of Demartini [28] and our results

Fig. 8 Comparison of simulated numerical and correlation results, variation of Nusselt number (Nu) and friction factor (f) versus Reynolds (Re) for a smooth channel

Results and discussion

The insertion of solid blocks (baffles) in a heat exchanger system causes disturbances in the flow and generates vortices that promote mixing of the heat transfer fluid, thus improving the heat transfer rate. Nevertheless, this increase in the transfer rate is always accompanied by pressure losses. So, the work presented in this paper aims in particular at the search for a configuration allowing an improvement in the thermohydrodynamic performance of the system with a minimum of pressure drop, i.e., it is necessary to increase the thermal improvement factor (η).

In order to study the possibility of improving the thermohydrodynamic performance of a heat exchange device, it is necessary to understand the thermal phenomenon and the dynamic behavior, which is translated by the nature of the flow structure and the value of the heat transfer rate. These two phenomena, thermal and dynamic, are always coupled and are influenced by the same parameters. For example, the location of a solid obstacle in the flow direction effectively affects its structure, and consequently, the heat exchange coefficient. Indeed, when the heat transfer fluid passes through the space limited by the top wall and the top of the baffle, which constitutes the attachment zone, the speed of the fluid particles is very high. We then observe the formation of two flow zones@[]. The first one, called the central zone, corresponds to the previous attachment zone, where the phenomenon is observed in the case (5) of Fig. 9. This zone is characterized by the fluctuation of the speed and intensity of the turbulence, which induces an intensification of thermal exchange and results in an increased heat transfer coefficient. A second zone, called the secondary recirculation zone, is located behind the deflector, and it is characterized by the birth of vortices that favor a mixing of

the different fluid flows and thus increase the heat transfer rates. Therefore, the flow structure in a heat exchange device and the transfer rate is directly related to the shape of the baffles inserted in the system duct. The improvement in the system's thermal performance by the insertion of the baffles naturally depends on its shape, position, and orientation. In order to carry out this analysis, different shapes of baffles are examined in this work. The positioning, inclination, and inter-baffle space are studied according to the different cases in Fig. 9 presented below. Cases 3, 4, 5, and 6 in Fig. 9 show that the inclination of the baffles actively contributes to the thermal and dynamic efficiency of a heat exchange system.

Figure 10a-d shows the influence of baffle placement and orientation on the hydrodynamic structure of the flow in terms of axial velocity profiles (variation of axial velocity along with the channel height). The curves presented represent the velocity profiles around the four baffles placed at the particular positions defined by: $x_1 = 0.2$ m; $x_2 = 0.255$ m; $x_3 = 0.285$ m and $x_4 = 0.315$ m. The Reynolds number chose to be equal to Re = 87.300. The different curves in Fig. 10 show the modification of the flow structure near the wall and the generation of vortices induced by the perturbations caused by the presence of the baffles, especially in the upper part of the channel. We can thus observe that the size of the vortices changes with the direction of the baffle's orientation. We also observe that when the fluid flow approaches a baffle, its velocity increases in the vicinity of the lower part of the channel. We note that the curves at the different positions have almost the same shape but with negative velocity values more marked in cases 2, 3, 4, and 5. Far from the baffle, since the fluid is not constrained, the flow is very intense, and after its passage in the downstream zone, it becomes less intense.

Figure 11a-d presents the streamlines and the temperature field in the plane of symmetry (x, y) in z = 0 at Re = 87 300 for different baffle orientations. One can observe the different zones where the baffles give rise to vortices along the channel, which generates a turbulence phenomenon that intensifies the heat exchange at the wall-fluid interface. On the other hand, it can be noticed that at the entrance of the channel, just upstream of the first baffle, there is the formation of dead zones where the fluid does not contribute to the flow. The sharp edge, located upstream of the baffle, presents a point of detachment. The flow is then detached from the wall of this one, which generates a depression downstream of this same baffle. The baffles in the direction of the flow within a heat transfer device make it possible to redirect the flow either toward the higher wall or toward, the lower wall. The first baffle directs the flow toward the bottom wall, while the second baffle directs it toward the top wall; this allows the fluid to capture all the thermal energy. This results in the appearance of the main flow and a secondary flow. The effects of the baffle on the flow structure and the heat
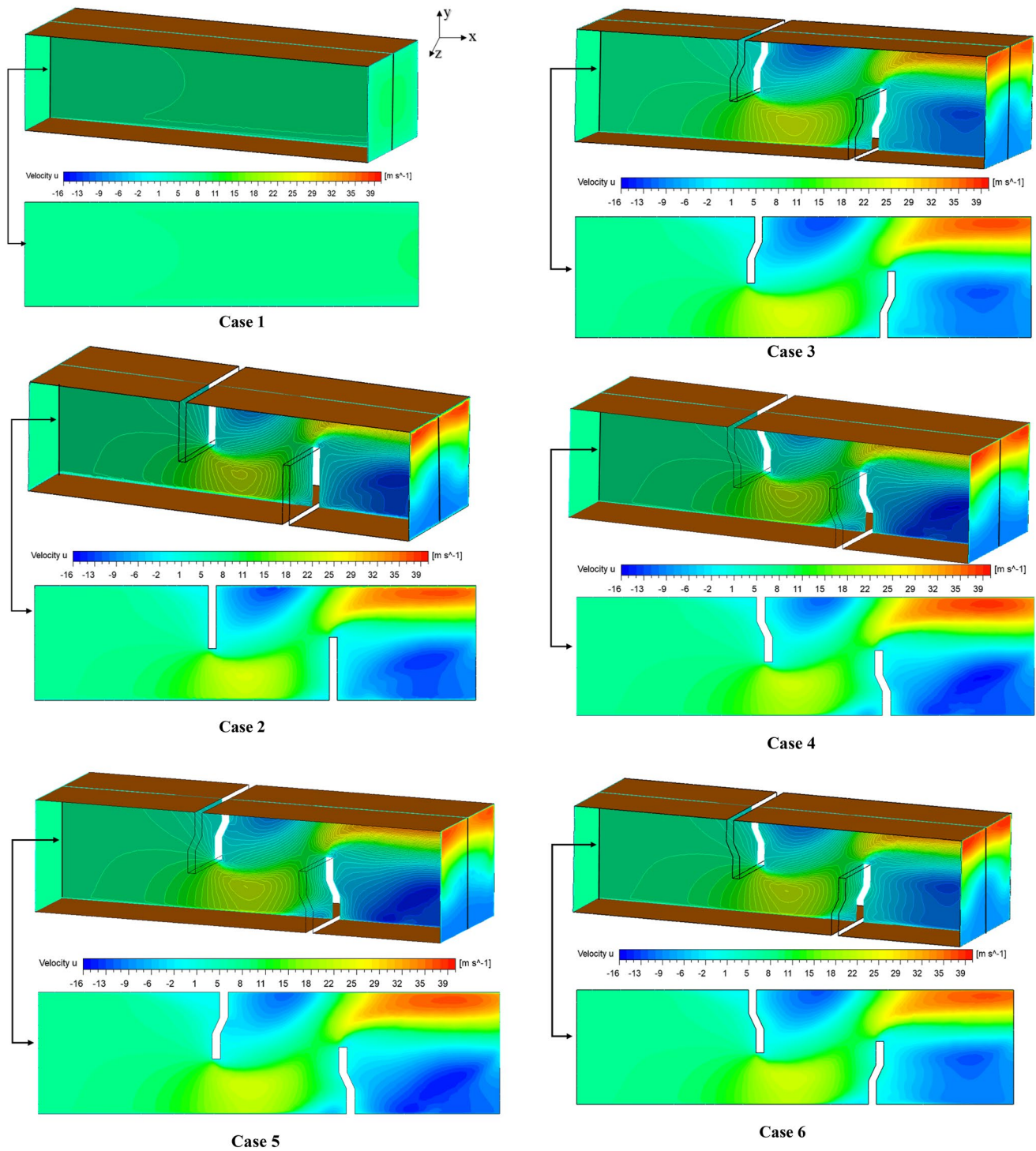
Fig. 9 Contours of the axial velocity [m/s] for Re = 87 300

exchange coefficient can be seen on the curves drawn in the transverse planes. The second baffle facilitates the flow of the fluid along the main direction of flow, thus decreasing the transverse component of the velocity and significantly reducing the length of attachment. This changing flow orientation allows the fluid to follow a very long path, which

creates a reasonably high vortex force within the flow and a more significant heat exchange coefficient.

The insertion of solid bodies (baffles) in the flow direction in a tubular channel induces disorientation of the flow accompanied by an intense fluctuation of the velocity. This causes solid local turbulence in the flow. The ovals
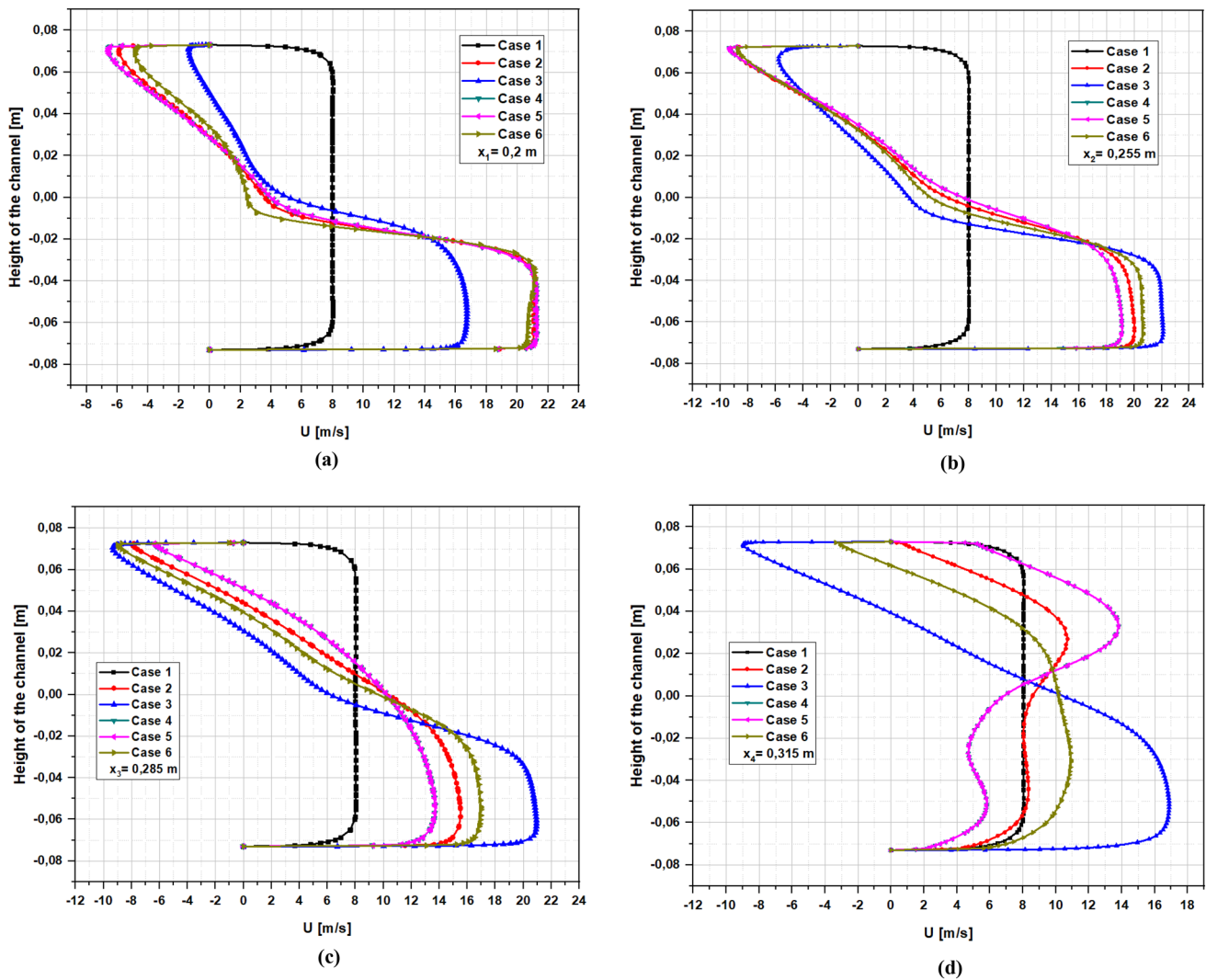
Fig. 10 Variation of the axial velocity at the four particular positions: **a** $x_1 = 0.2$ m; **b** $x_2 = 0.255$ m; **c** $x_3 = 0.285$ m; **d** $x_4 = 0.315$ m

represented in Fig. 12 show the distribution of the kinetic energy of the turbulence for the six cases studied. We find that, unlike the case of the tubular channel without baffles, in the device with baffles, the flow is characterized by a considerable turbulence kinetic energy, indicating that the fluid flow in the duct is entirely turbulent overall. Thus, the thickness of the thermal resistance layer decreases, the deposition of particles on the channel surface cannot take place, and the heat exchange improves.

Figure 13a-d illustrates the temperature profiles of the fluid for a given Reynolds number equal to 87,300, which is calculated for different cross sections of the channel: x = 0.2, 0.255, 0.285, and 0.315 m.

The analysis of the results represented by the different graphs show that, in each cross section, the more the axial speed of the fluid increases, the more its temperature decreases. That is to say that they are inversely proportional.

It is also observed that the sections closer to the baffle are more heated than the distant vertical sections. This finding is consistent with the observation about the channel's temperature field distribution.

Figure 14 represents the evolution of the average Nusselt number (Nu) as a function of the Reynolds number for different geometric cases. The variation of the Reynolds number is chosen in the same range (10,000 and 87,300) for all geometric configurations. It is observed that in all cases, the curves have the same slope. In other words, the values of the Nusselt number increase proportionally with increasing Reynolds numbers. Thus, the higher the Reynolds number of the flow, the higher the heat transfer coefficient, and a significant improvement of the system's thermal performance is observed.

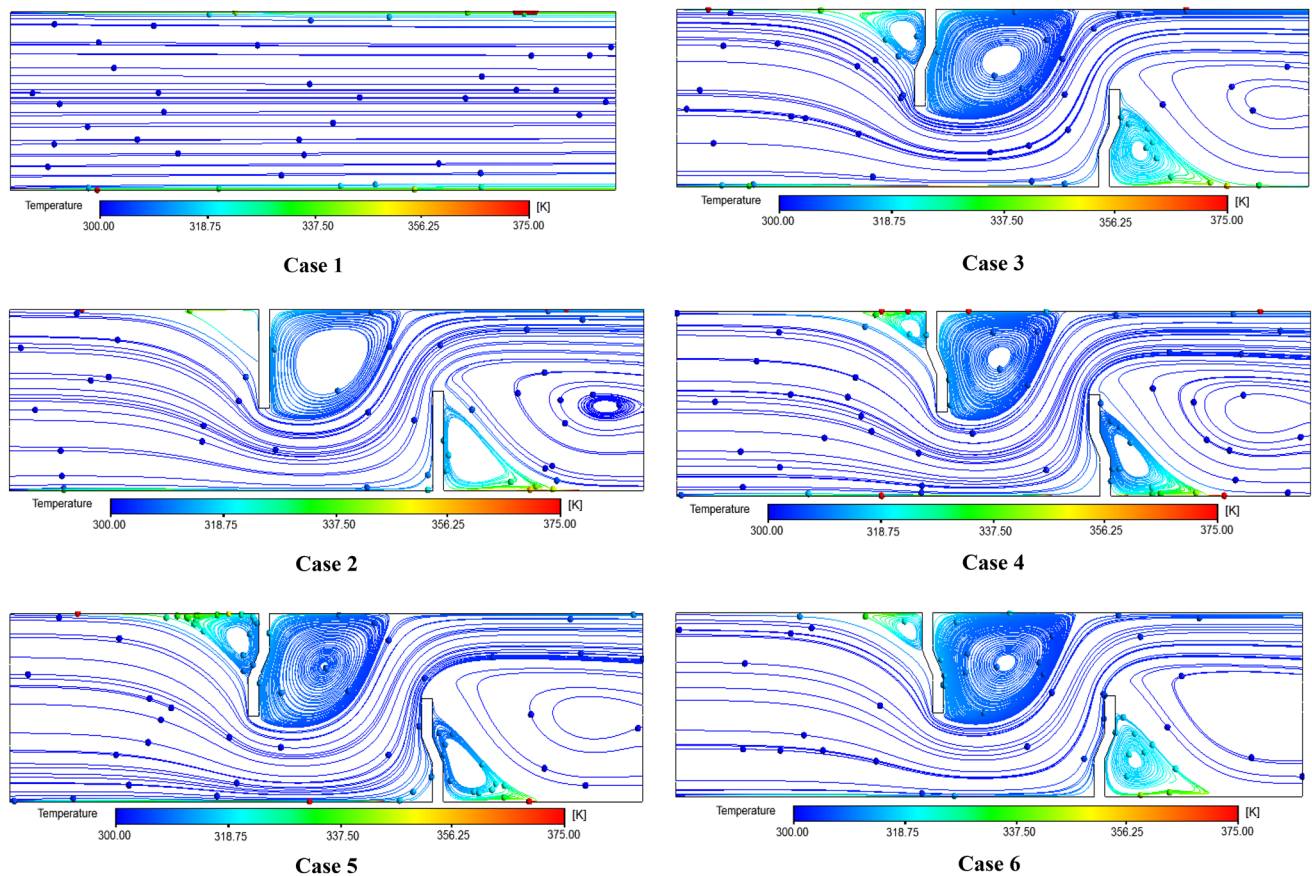It is more logical to note that any increase in heat transfer results from an increase in friction between the

Fig. 11 Streamlines and isotherms [K°] for Re = 87 300

particles, therefore an increase in the friction coefficient leading to a loss of pressure. In Fig. 15, we have represented the variation of the friction factor as a function of the Reynolds number for the different cases that we have considered. However, according to the analysis of the results, in comparison with the smooth channel without baffle, the insertion of the baffles increases the friction, but the insertion of the partially inclined baffles proves to be the most optimal technique to acquire the best friction factor. Moreover, for a Reynolds number equal to 10,000, the percentage of the friction factor for the different cases studied: (2); (3); (4); (5) and (6), the percentage of friction factor is equal to 32.37%; 30.35%; 37.09%; 37.15%; and 26.41%, respectively. It can conclude that the formation of vortices in the downstream area of the baffles is the cause of the pressure drop observed inside the channel, while the presence of the incline contributes to the elimination of vortices behind the baffles, thus reducing the pressure drop.

The Nusselt number/friction factor correlations presented in Tables 5 and 6 are valid for a fixed Prandtl number, and the Reynolds number varies between 10,000 and 87,300 and formulates from the results in Figs. 14 and 15.

In Fig. 16, the variation of the thermal performance enhancement factor (TEF) as a function of Reynold's number (Re) for the cases considered in this study. From the data obtained from Nu and f, it is observed that the values of the thermal performance enhancement factor (TEF) tend to decrease with increasing values of Reynolds number (Re) for all the cases analyzed. On the other hand, for a Reynolds number fixed at the value 87,300, the values of the factor (TEF) are, respectively, equal to 2.18; 2.16; 2.19; 2.27; and 2.25, respectively, for the different cases studied: (2); (3); (4); (5); and (6). In addition, it can see that the value of TEF corresponding to case (5) is higher than that of the other cases studied. Therefore, the geometrical configuration corresponding to case (5) can be chosen and adapted to improve heat the thermal performance for heat transfer inside the channel.

The curves in Fig. 17 illustrate the evolution of the quantity of heat transmitted as a Reynolds number (Re) function for the different cases studied. The results obtained show that the amount of heat transmitted by the system is proportional to the increase of the Reynolds number. We find that for the cases studied, case (2), case (3), case (4), case (5), and case (6), relative to the
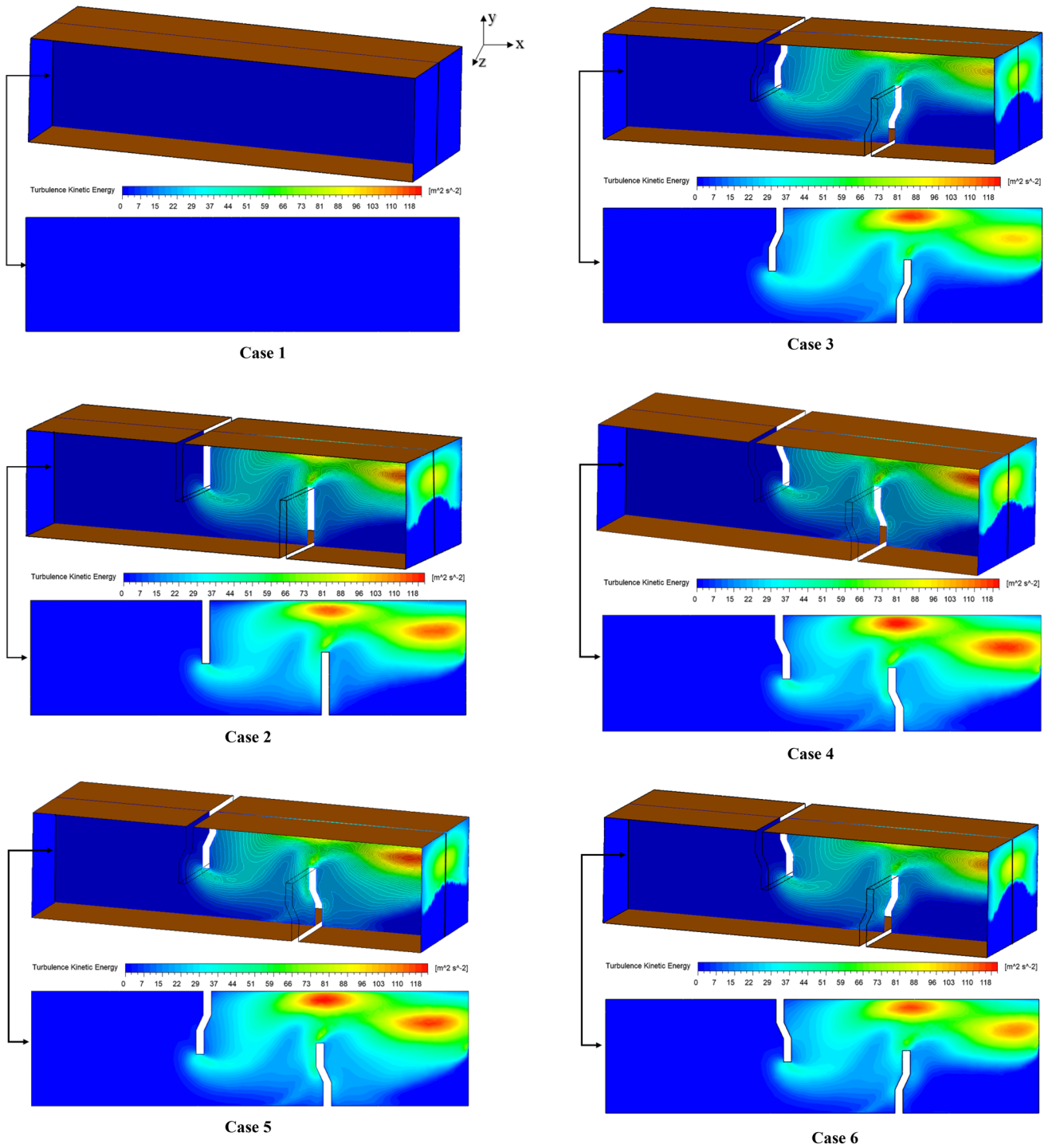
Fig. 12 Turbulent kinetic energy (m²/s²)

smooth case and for the exact value of Reynold's number 87300, the relative heat quantities transmitted are, respectively, equal to, 116.08%, 113.93%, 118.2%, 121.71, and 109.39%. Furthermore, we can say that the configuration corresponding to case (5) is more efficient for heat transfer than the others.

Comparison with previous works

By comparing our results to literature results calculated by other models (Fig. 17); one with four baffles (yellow), and the second with ten baffles (purple), for a Reynolds number around 12,000, we could see that the configuration
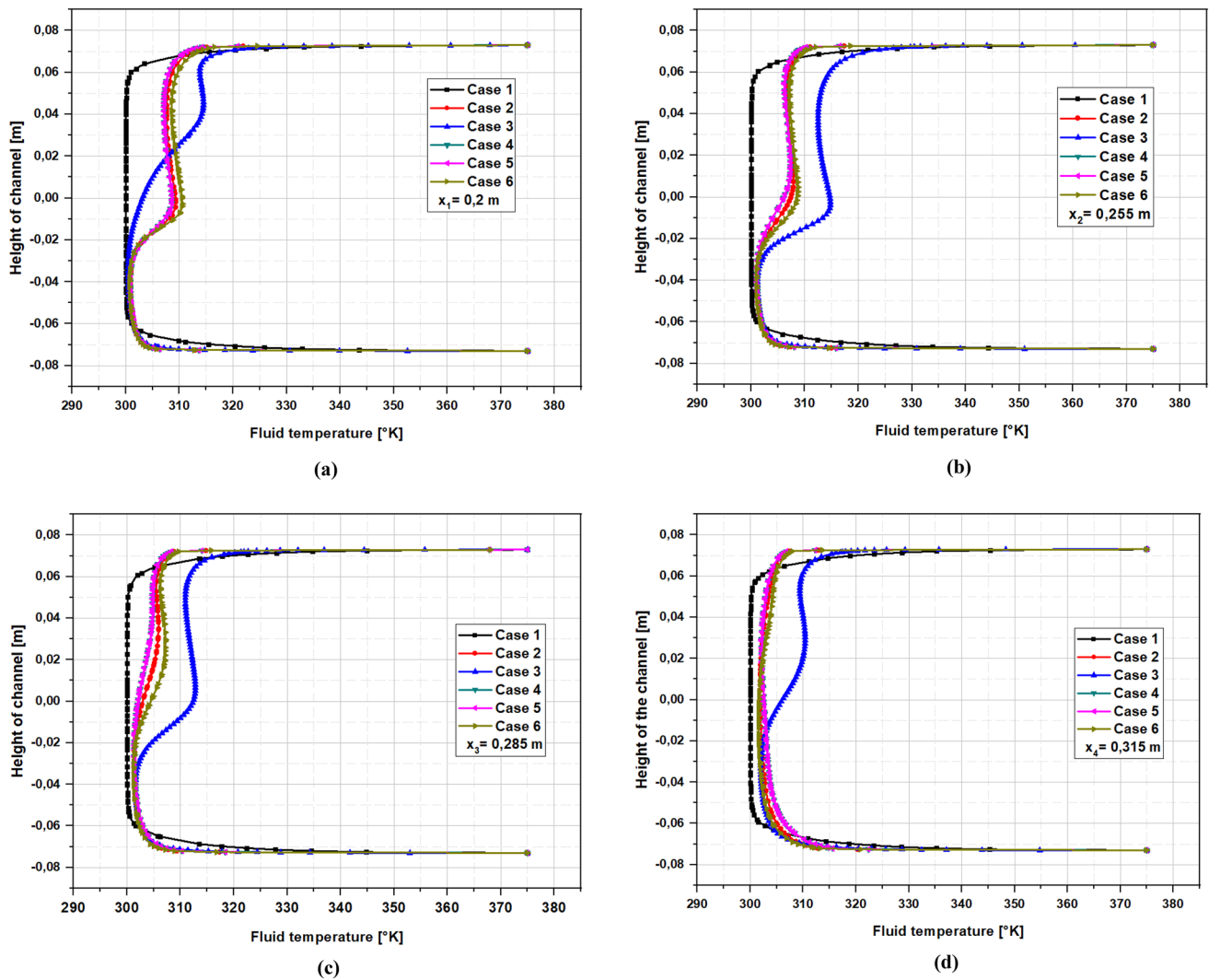
Fig. 13 Temperature profile

corresponding to case (5) (with two partially inclined and orientable baffles) are more optimal to make the heat exchanger more efficient (Table 7).

Conclusion

This study aimed to investigate the impact of a novel baffle configuration on enhancing heat transfer for the duct. The system studied is a rectangular channel equipped with two baffles placed in different positions and orientations and crossed by a turbulent flow of a heat transfer fluid.

The results of this analysis show that:

- The baffles' presence generates vortex flows that effectively act on the flow characteristics and heat exchange, resulting in intensifying heat exchange at the fluid-wall separation surface.
- The baffle inclination's presence contributes to eliminating vortices behind the baffles, which reduces the pressure drop. In all cases, inclined baffles perform better than straight baffles.
- The results also indicate that the thermal performance enhancement factor (TEF) is more significant in case (5). Therefore, the configuration corresponding to this case performs better in heat transfer than in the other cases.
- In perspective, a combined heat exchanger analysis with inclined baffles with differently arranged perforations is proposed.
- The relative heat transfers for case 5 are equal to 121%, but the friction factor is only increased by 37%, which shows that it is the most optimal configuration to improve the system in terms of heat transfer.
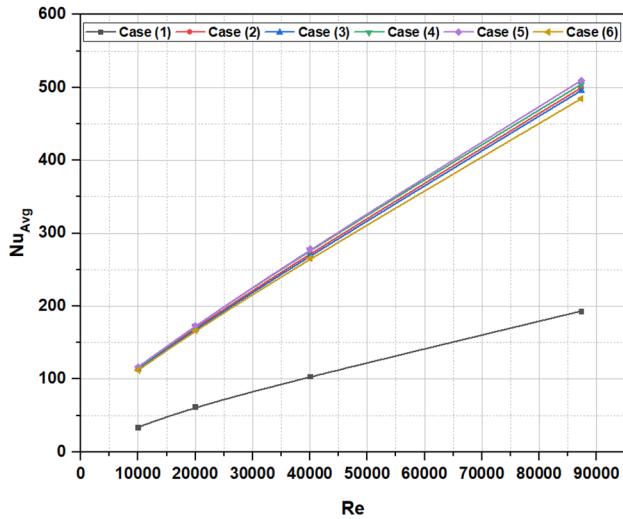
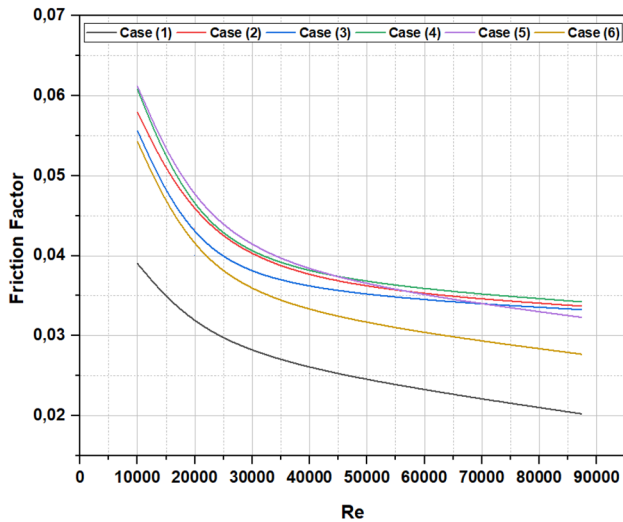**Fig. 14** Variation of the average Nusselt number as a function of the Reynolds number for different cases

Fig. 15 Variation of the friction factor with Reynolds number for different cases

Table 5 Average Nusselt number

	Nu_{Avg}	R^2
Case (1)	$Nu_{Avg} = 0,002(Re) + 18,848$	0.9965
Case (2)	$Nu_{Avg} = 0,0049(Re) + 69,694$	0.9994
Case (3)	$Nu_{Avg} = 0,0049(Re) + 68,603$	0.9995
Case (4)	$Nu_{Avg} = 0,005(Re) + 71,432$	0.999
Case (5)	$Nu_{Avg} = 0,0051(Re) + 70,767$	0.9993
Case (6)	$Nu_{Avg} = 0,0048(Re) + 68,892$	0.9993

Table 6 Friction factor (f)

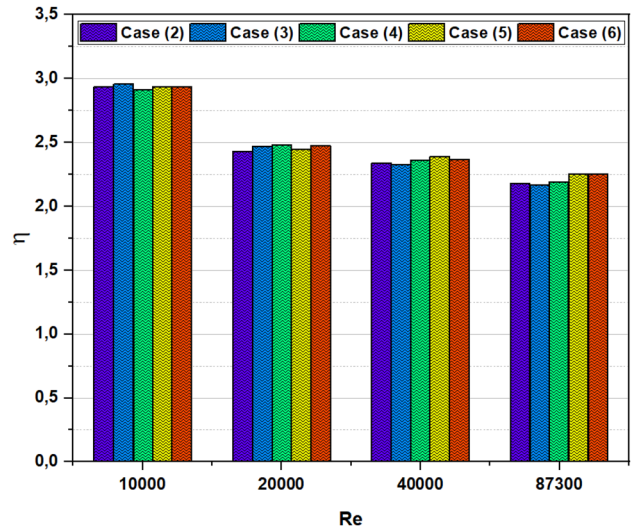|	Friction factor (f)	R^2
Case (1)	$f = 5E{-}12(Re)^2 - 7E{-}07(Re) + 0,0443$	0,9716
Case (2)	$f = 9E{-}12(Re)^2 - 1E{-}06(Re) + 0,0667$	0,9467
Case (3)	$f = 9E{-}12(Re)^2 - 1E{-}06(Re) + 0,0631$	0,8949
Case (4)	$f = 1E{-}11(Re)^2 - 1E{-}06(Re) + 0,0698$	0,9144
Case (5)	$f = 1E{-}11(Re)^2 - 1E{-}06(Re) + 0,0706$	0,9466
Case (6)	$f = 9E{-}12(Re)^2 - 1E{-}06(Re) + 0,0626$	0,9341

Fig. 16 The variation of the thermal performance enhancement factor (TEF) as a function of Reynolds number
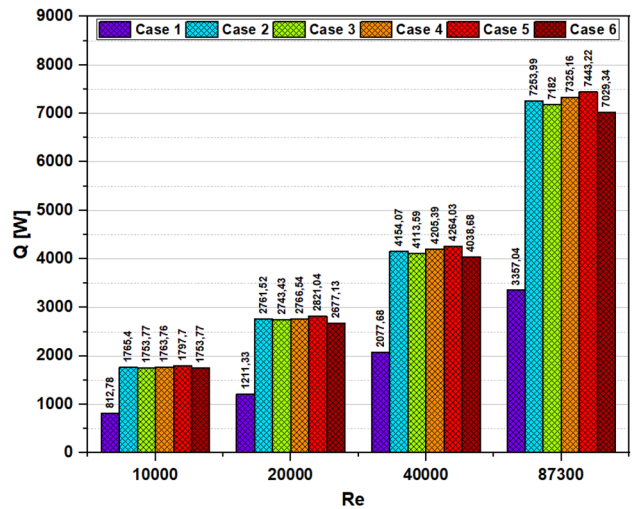

Fig. 17 Variation of the quantity of heat transmitted Q

Table 7 Benchmark of thermal–hydraulic performance parameters for the same Reynolds number (Re = 12,000) compared to prior studies

investigators	configuration	Thermo-hydraulic performance parameter
Present Study	Case (5): channel with two partially inclined baffles	2.85
Sahel et al. [40]	Channel with ten Simple-baffles	3.05
Menni et al. [41]	Channel with four V-baffles	1.67

- New correlations for predicting the friction factor and Nusselt number as a function of the Reynolds number and the configuration developed at the end of this analysis.
- The proposed case (5) has a thermal performance of 2.85, which is 70.65% more performant than the proposed V-shape baffles.

Author contributions JES performed, analyzed and interpreted data and results.TZ analyzed and interpreted data and results. NH analyzed and interpreted data and results. MS was a major contributor in writing the manuscript. NS was a major contributor in writing the manuscript. MC analyzed and interpreted data and results.

Funding Not applicable.

Data availability Not applicable.

Declarations

Conflict of interest The authors declare that they have no conflict of interest.

Ethical Approval Not applicable.

References

1. Ismael, M.A., Jasim, H.F.: Role of the fluid-structure interaction in mixed convection in a vented cavity. Int. J. Mech. Sci. **135**, 190–202 (2018). https://doi.org/10.1016/j.ijmecsci.2017.11.001
2. Sabbar, W.A., Ismael, M.A., Almudhafar, M.: Fluid-structure interaction of mixed convection in a cavity-channel assembly of flexible wall. Int. J. Mech. Sci. **149**, 73–83 (2018). https://doi.org/10.1016/j.ijmecsci.2018.09.041
3. Alsabery, A.I., Sheremet, M.A., Ghalambaz, M., Chamkha, A.J., Hashim, I.: Fluid structure interaction in natural convection heat transfer in an oblique cavity with a flexible oscillating fin and partial heating. Appl. Therm. Eng. **145**, 80–97 (2018). https://doi.org/10.1016/j.applthermaleng.2018.09.039
4. Mehryan, S.A., Ghalambaz, M., Ismael, M.A., Chamkha, A.J.: Analysis of fluid-solid interaction in MHD natural convection in a square cavity equally partitioned by a vertical flexible membrane. J. Magn. Magn. Mater. **424**, 161–173 (2017). https://doi.org/10.1016/j.jmmm.2016.09.123
5. Ghalambaz, M., Jamesahar, E., Ismael, M.A., Chamkha, A.J.: Fluid-structure interaction study of natural convection heat transfer over a flexible oscillating fin in a square cavity. Int. J. Therm. Sci. **111**, 256–273 (2017). https://doi.org/10.1016/j.ijthermalsci.2016.09.001
6. Khetib, Y., Sait, H., Habeebullah, B., Hussain, A.: Numerical study of the effect of curved turbulators on the exergy efficiency of solar collector containing two-phase hybrid nanofluid. Sustain. Energy Technol. Assess. **47**, 101436 (2021). https://doi.org/10.1016/j.seta.2021.101436
7. Salhi, J.E., Zarrouk, T., Salhi, N.: Numerical analysis of the properties of nanofluids and their impact on the thermohydrodynamic phenomenon in a heat exchanger. Mater. Today: Proceed. **45**, 7559–7565 (2021). https://doi.org/10.1016/j.matpr.2021.02.365
8. Salhi, J.E., Zarrouk, T., Salhi, N.: Numerical study of the thermo-energy of a tubular heat exchanger with longitudinal baffles. Mater. Today: Proceed. **45**, 7306–7313 (2021). https://doi.org/10.1016/j.matpr.2020.12.1213
9. Menni, Y., Ameur, H., Sharifpur, M., Ahmadi, M.H.: Effects of in-line deflectors on the overall performance of a channel heat exchanger. Eng. Appl. Comput. Fluid Mech. Bose. **15**(1), 512–529 (2021). https://doi.org/10.1080/19942060.2021.1893820
10. Siddiqui, M.K.: Heat transfer augmentation in a heat exchanger tube using a baffle. Int. J. Heat Fluid Flow **28**(2), 318–328 (2007). https://doi.org/10.1016/j.ijheatfluidflow.2006.03.020
11. Menni, Y., Azzi, A., Chamkha, A.J., Harmand, S.: Effect of wall-mounted V-baffle position in a turbulent flow through a channel: Analysis of best configuration for optimal heat transfer. Int. J. Numer, Methods Heat Fluid Flow. **29(10)**, 3908–3937 (2019). https://doi.org/10.1108/HFF-06-2018-0270
12. Salhi, J.E., Amghar, K., Filali, A., Salhi, N.: ffect of the Spacing Design of Two Alternate Baffles on the Performance of Heat Exchangers. Defect and Diffusion Forum. **415,** 53–72 (2022). https://doi.org/10.4028/p-826179
13. Salhi, J.E., Salhi, N.: Three-Dimensional Analysis of the Effect of Transverse Spacing between Perforations of a Deflector in a Heat Exchanger. International Conference on Electronic Engineering and Renewable Energy Springer. 719–728 (2020). https://doi.org/10.1007/978-981-15-6259-4_75
14. Salahuddin, U., Bilal, M., Ejaz, H.: A review of the advancements made in helical baffles used in shell and tube heat exchangers. Int. Commun. Heat Mass Transfer **67**, 104–108 (2015). https://doi.org/10.1016/j.icheatmasstransfer.2015.07.005
15. Nedunchezhiyan, M., Karthikeyan, R., Ramalingam, S., Damodaran, D., Ravikumar, J., Sampath, S., Kaliyaperumal, G.: Influence Of Baffles In Heat Transfer Fluid Characteristics Using Cfd Evaluation. International Journal of Ambient Energy. 1–29 (2022). https://doi.org/10.1080/01430750.2022.2063175
16. Salhi, J.E., ES-Sabry, Y., El Hour, H., Salhi, N.: Numerical analysis of the thermal performance of a nanofluid water-Al$_2$O$_3$ in a heat sink with rectangular microchannel. 2nd International conference on Electronics, Control, Optimization and Computer Science. IEEE. 1–6 (2020). https://doi.org/10.1109/ICECOCS50124.2020.9314421
17. Ismael, M.A.: Forced convection in partially compliant channel with two alternated baffles. International Journal of Heat and Mass Transfer. **142**, 118455 (2019). https://doi.org/10.1016/j.ijheatmasstransfer.2019.118455
18. Salhi, J.E., Amghar, K., Bouali, H., Salhi, N.: Combined Heat and Mass Transfer of Fluid Flowing through Horizontal Channel by

Turbulent Forced Convection. Modeling and Simulation in Engineering. 1–11 (2020). https://doi.org/10.1155/2020/1453893

19. Kelkar, K.M., Patankar, S.V.: Numerical prediction of flow and heat transfer in a parallel plate channel with staggered fins. **09(1)**, 25–30 (1987). https://doi.org/10.1115/1.3248058

20. Maakoul, A.E.I., Laknizi, A., Saadeddine, S., Metoui, M.E.I., Zaite, A., Meziane, M., Ben Abdellah, A.: Numerical comparison of shell-side performance for shell and tube heat exchangers with trefoil-hole, helical and segmental baffles. Appl. Therm. Eng. **109** (Part A), 175–185 (2016). https://doi.org/10.1016/j.applthermaleng.2016.08.067

21. Lei, Y.G., He, Y.L., Li, R., Gao, Y.F.: Effects of baffle inclination angle on flow and heat transfer of a heat exchanger with helical baffles. Chem. Eng. Process. **47(12)**, 2336–2345 (2008). https://doi.org/10.1016/j.cep.2008.01.012

22. Sahel, D., Ameur, H., Benzeguir, R., Kamla, Y.: Enhancement of heat transfer in a rectangular channel with perforated baffles. App. Therm. Eng. **101**, 156–164 (2016). https://doi.org/10.1016/j.applthermaleng.2016.02.136

23. Sara, O.N., Pekdemir, T., Yapici, S.: Enhancement of heat transfer from a flat surface in a channel flow by attachment of rectangular blocks. Int. J. Renew. Energy Res. **25**(7), 563–576 (2001). https://doi.org/10.1002/er.703

24. Chai, L., Xia, G.D., Wang, H.S.: Numerical study of laminar flow and heat transfer in microchannel heat sink with offset ribs on sidewalls. App. Therm. Eng. **92**, 32–41 (2016). https://doi.org/10.1016/j.applthermaleng.2015.09.071

25. Chang, S.W., Chen, T.W., Chen, Y.W.: Detailed heat transfer and friction factor measurements for square channel enhanced by plate insert with inclined baffles and perforated slots. App. Therm. Eng. **159**, 113856 (2019). https://doi.org/10.1016/j.applthermaleng.2019.113856

26. Vashistha, C., Patil, A.K., Kumar. M.: Experimental investigation of heat transfer and pressure drop in a circular tube with multiple inserts. App. Therm. Eng. **96**, 117–129 (2016). https://doi.org/10.1016/j.applthermaleng.2015.11.077

27. Gunes, S., Ozceyhan, V., Buyukalaca, O.: The experimental investigation of heat transfer and pressure drop in a tube with coiled wire inserts placed separately from the tube wall. Appl. Therm. Eng. **30**, 1719–1725 (2010). https://doi.org/10.1016/j.applthermaleng.2010.04.001

28. Demartini, L.C., Vielmo, H.A., Möller, S.V.: Numeric and experimental analysis of the turbulent flow through a channel with baffle plates. J. Braz. Soc. Mech. Sci. Eng. **26**(2), 153–159 (2004). https://doi.org/10.1590/S1678-58782004000200006

29. Feijó, B.C., Lorenzini, G., Isoldi, L.A., Rocha, L.A.O., Goulart, J.N.V., dos Santos, E.D.: Constructal design of forced convective flows in channels with two alternated rectangular heated bodies. Int. J. Heat Mass Transf. **125**, 710–721 (2018). https://doi.org/10.1016/j.ijheatmasstransfer.2018.04.086

30. Bazdidi-Tehrani, F., Naderi-Abadi, M.: Numerical analysis of laminar heat transfer in entrance region of a horizontal channel with transverse fins. Int. Commun. Heat Mass Transf. **31**, 211–220 (2004). https://doi.org/10.1016/S0735-1933(03)00226-4

31. Chieng, C.C., Launder, B.E.: On the calculation of turbulent heat transport downstream from an abrupt pipe expansion. Numer. Heat Transf. **3**(2), 189–207 (1980). https://doi.org/10.1080/01495728008961754

32. Launder, B.E., Spalding, D.B.: The numerical computation of turbulent flows. Comput. Methods Appl. Mech. Eng. **3**, 269–289 (1974). https://doi.org/10.1016/B978-0-08-030937-8.50016-7

33. Patankar, S.V.: Numerical Heat Transfer and Fluid Flow. Series in Computational Methods in Mechanics and Thermal Sciences, Hemi-sphere, New York. (1980).

34. Salhi, J.E., Zarrouk, T., Merrouni, A.A., Salhi, M., Salhi, N.: Numerical investigations of the impact of a novel turbulator configuration on the performances enhancement of heat exchangers. J. Energy Storage. **46**, 103813 (2022). https://doi.org/10.1016/j.est.2021.103813

35. Salhi, J.E., Salhi, M., Amghar, K., Zarrouk, T., Salhi, N.: Analysis of the thermohydrodynamic behavior of a cooling system equipped with adjustable fins crossed by the turbulent flow of air in forced convection. Int. J. Energy Env. Eng.. 1–13 (2021). https://doi.org/10.1007/s40095–021–00446–5

36. Leonard, B.P., Mokhtari, S.: Ultra-Sharp nonoscillatory convection schemes for High-Speed steady multidimensional flow. NASA TM 1–2568, NASA Lewis Research Center. (1990).

37. Dittus, F.W., Boelter, L.M.K.: Publications on engineering. University of California, Berkeley. **2**, 443 (1930).

38. Moody, L.F.: Friction factors for pipe flow. Trans. Asme. **66**, 671–684 (1944).

39. ANSYS Inc. ANSYS Fluent Theory Guide 19.0 (2018).

40. Sahel, D., Ameur, H., Baki, T.: Effect of the size of graded baffles on the performance of channel heat exchangers. Thermal Sci.. **24**(2 Part A), 767–775 (2020). https://doi.org/10.2298/TSCI180326295S

41. Menni, Y., Ghazvini, M., Ameur, H., Ahmadi, M. H., Sharifpur, M., Sadeghzadeh, M.: Numerical calculations of the thermal-aerodynamic characteristics in a solar duct with multiple V-baffles. Eng. Appl. Comput. Fluid Mech. **14**(1), 1173–1197 (2020). https://doi.org/10.1080/19942060.2020.1815586